

# Aerodynamic behaviour of NREL S826 airfoil at Re=100,000

**Chivaee, Hamid Sarlak; Mikkelsen, Robert Flemming; Sarmast, Sasan; Sørensen, Jens Nørkær**

*Published in:*
Journal of Physics: Conference Series (Online)

*Link to article, DOI:*
10.1088/1742-6596/524/1/012027

*Publication date:*
2014

*Document Version*
Publisher's PDF, also known as Version of record

Aerodynamic behaviour of NREL S826 airfoil at Re=100,000



2014 J. Phys.: Conf. Ser. 524 012027

(http://iopscience.iop.org/1742-6596/524/1/012027)

# Aerodynamic behaviour of NREL S826 airfoil at Re=100,000

**H Sarlak[1], R Mikkelsen[1], S Sarmast[1,2], JN Sørensen[1]**

[1] Technical University of Denmark, DK-2800 Lyngby, Denmark.

[2] Swedish e-Science Research Centre (SeRC), Linne FLOW Centre, KTH Mechanics, Royal Institute of Technology, SE-100 44 Stockholm, Sweden.

E-mail: hsar@dtu.dk

**Abstract.** This paper presents wind tunnel measurements of the NREL S826 airfoil at Reynolds number $Re = 100,000$ for angles of attack in a range of $-10^o$ to $25^o$, and the corresponding Large Eddy Simulation (LES) for selected angles of attack.

The measurements have been performed at the low speed wind tunnel located at Fluid Mechanics laboratory of the Technical University of Denmark (DTU). Lift coefficient is obtained from the forge gauge measurements while the drag is measured according to the integration of the wake profiles downstream of the airfoil. The pressure distribution is measured by a set of pressure taps on the airfoil surface.

The lift and drag polars are obtained from the LES computations using DTU's in-house CFD solver, EllipSys3D, and good agreement is found between the measurement and the simulations. At high angles of attack, the numerical computations tend to over-predict the lift coefficients, however, there is a better agreement between the drag measurements and computations. It is concluded that LES computations are able to capture the lift and drag polars as well as the pressure distribution around the airfoil with an acceptable accuracy.

## 1. Introduction

Recently, a series of blind test comparisons on measurements of a model scale wind turbine was conducted in a low speed wind tunnel facility at Norwegian University of Science and Technology (NTNU), with several researchers invited to perform numerical simulations and predict the rotor performance and wake characteristics. The design Reynolds number for the rotor airfoil sections was of the order of $Re = 100,000$ and

one of the challenges of performing the comparison with the experimental results was the lack of accurate tabulated airfoil data at such Reynolds numbers. Therefore, a wind tunnel measurement campaign was concucted in DTU's Fluid Mechanics laboratory to obtain the required lift and drag polars. The campaign was extended to include pressure measurements on the airfoil surface as well. Moreover, a numerical study was carried out to quantify capability of LES in predicting the pressure distribution as well as the lift and drag coefficients.

Wind tunnel measurements for the sake of finding airfoil characteristics have been widely investigated throught the years [1, 2, 3]. LES, on the other hand, is a rather new technique and has not been of high interest for the airfoil computations due to its high computational expense. Nevertheless, recent studies have proved its capability for airfoil simulations [11], thanks to increased computational power and elaboration of LES techniques. Recently, a study was performed with the aim of investigating the potential of LES in predicting the airfoil characteristics at high Reynolds numbers [10]. The study included simulations of the flow around an Aerospatiale A-airfoil at $Re = 2 \times 10^6$ and an angle of attack $\alpha = 13.3^o$. Different aspects of the simulations were investigated, such as the effects of the mesh resolution, size of the computational domain, sub-grid scale (SGS) modeling, near-wall treatment, and transition prediction. It was concluded that the mesh resolution and the numerical span width have a significant impact on predicting an accurate flow. Eisenbach and Friedrich [21] conducted LES of a NACA 4415 profile placed between two flat plates at $\alpha = 18^o$ using the dynamic Smagorinsky model and an immersed boundary method for treatment of the wall. Uranga et al. [4] performed LES of the flow over a Selig-Donovan SD7003 airfoil for a range of Reynolds numbers between $10,000$ and $60,000$ at $\alpha = 13.3^o$ using a high-order discontinuous Galerkin method. They used an implicit LES modeling, in which the effect of the SGS model is applied through the numerical dissipation of the discretization schemes. Ying and Wang [18] used an implicit model to simulate the flow around SD7003 airfoil at $Re = 60,000$ using a high-order spectral difference method. The SD7003 airfoil was chosen in all cases because of the availability of the experimental data [2]. Recent investigations of the airfoil flow is reported by Venugopal et al. [16] who performed an LES of a DU96 airfoil at the near-stall angle of attack at $Re = 1.5 \times 10^6$.

## 2. Experimental set-up

The experiments are performed at the Fluid Mechanics laboratory at the Technical University of Denmark. The incompressible, low speed, open-loop wind tunnel facility shown in figure 1 has a cross section of $0.5m \times 0.5m$, a contraction ratio of $1 : 12.5$, and a maximum speed-up capability of $U_\infty = 65m/s$. The turbulence intensity of the empty

wind tunnel is 0.22% at $U_\infty = 15m/s$, corresponding to a chord Reynolds number of 100,000 for the airfoil considered in the measurements. The intensity drops to 0.15% at $U_\infty = 50m/s$. Surface pressure is measured using 30 pressure tabs along the chord of the tested airfoil model. The dash-lines shown on the figure 1 are not instrumented. Instead, the pressure data for the second point in the pressure side from the trailing edge (TE) and the first point from the leading edge (LE) are extrapolated from their two neighbouring points (the same side) and the pressure in the TE is interpolated from the second points in the pressure and suction sides. The airfoil has a chord and span of of 100 and 500 milimeters, respectively. The lift coefficients are measured using load cells and the drag coefficient is obtained by the wake rake measurements placed $1.6c$ downstream of the airfoil. The angle of attack is set by means of a servo motor.

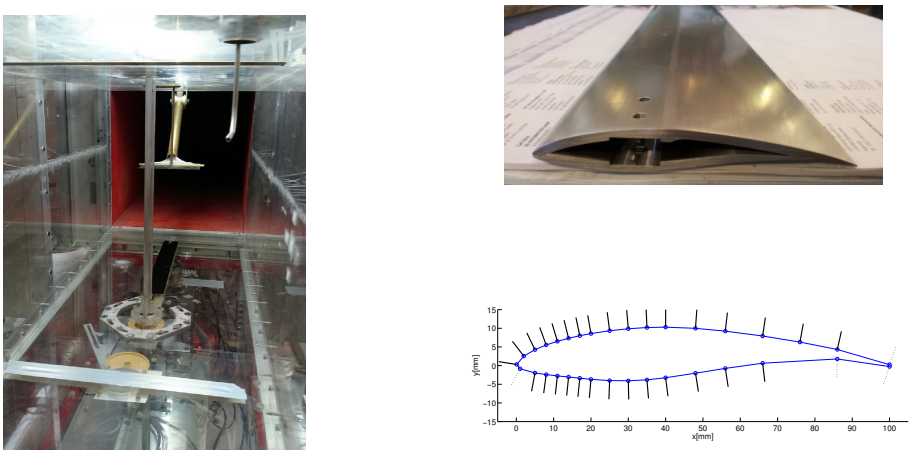


**Figure 1:** (left) Wind tunnel test section. (right) The CNC-machined S826 airfoil and the pressure tap locations.

Pressure measurements are performed with a sampling frequency of $125Hz$ for a duration of 10 sec at each angle of incidence in the upstroke (from -10 to +25) as well as downstroke (+25 to -10) pitching of the airfoil. The jump from each angle to the next one is performed using a step function and the corresponding recorded data are removed to ensure independence from the transition period. More information on the experimental set-up and a full set of benchmarks can be found in Sarlak [8].

## 3. The numerical simulation set-up

For the numerical simulations, the block structured general purpose flow solver Ellipsys3D, developed by Sørensen [7] and Michelsen [6] is used. In EllipSys3D, the incompressible Navier-Stokes equations are discretized using a finite volume method for the primitive variables (velocity and pressure). Discretization of the diffusive terms is

handled by $2^{nd}$ order central differencing schemes (CDS) and for the convective terms, a blend of CDS and QUICK scheme, is used for the purpose of numerical stability and accuracy. Time is discretized using a second order backward Euler scheme and the solution is marched in time using inner time stepping where the number of each pseudo time step can be either specified or remain as a function of the residuals. Pressure checker-boarding is prevented by using Rhie-Chow interpolation [17] on a collocated grid arrangement and the pressure correction equation is solved using PISO algorithm. The filtered Navier-Stokes equation reads in its vectorized form as

$$\frac{\partial \mathbf{v}}{\partial t} + \mathbf{v} \cdot \nabla \mathbf{v} \quad = \quad -\frac{\nabla p}{\rho} + \nabla \cdot [(\nu + \nu_{sgs}) \nabla \mathbf{v}] + \frac{\mathbf{f}}{\rho}, \tag{1}$$

where $\rho$ and $\nu$ are the fluid density and kinematic viscosity respectively. $\mathbf{v}$ represents the filtered velocity vector, $p$ is the modified pressure, and $\mathbf{f}$ is the external body force acting on the flow due to the presence of the wind turbine. $\nu_{sgs}$ is the eddy viscosity to be specified by the SGS model. The mixed scale SGS model (MO) by [13] was chosen for all of the test cases. In the MO model, the eddy viscosity is modeled as $\nu_{sgs} = c_{mo}\Delta^{1.5} q_c^{0.25} |\bar{\Omega}|^{0.5}$ using $c_{mo} = 0.01$, where $\Delta(i,j,k) = (dx.dy.dz)^{\frac{1}{3}}$ is the implicit filter width, $q_c$ is the SGS kinetic energy obtained with an explicit filtering and $\Omega$ is the vorticity vector magnitude. The simulations have been performed on two types of grid as shown in figure 2. A traditional C-mesh was used to perform simulations at low angles of attack while for higher angles of attack, a hybrid mesh consisting of O and H-mesh configurations, called the Tunnel mesh hereafter, was used in a numerical wind tunnel. The Tunnel grid is similar to the the experimental wind tunnel's test section but with a smaller span width. The flow is always parallel to the $X$ coordinate and the airfoil is rotated to set angles of attack.

To have the least dissipation error from the time discretizaton method, a non-dimentional time step of $dt^* = dtU_0/c$ is chosen to ensure that the CFL number is kept below 1, although an implicit time stepping is used. To choose the mesh size, the skin friction is first estimated according to empirical relations (e.g. $C_f = [2\,log_{10}(Re_x) - 0.65]^{-2.3}$ for $Re_x \leq 10^9$ [19]), wall shear stress defined as $\tau_w = C_f \cdot \frac{1}{2}\rho U_\infty^2$ and the friction velocity determined from $u_\tau = \sqrt{\frac{\tau_w}{\rho}}$. Finally, the desired grid spacing is computed according to the wall units $y = y^+ \mu / \rho\, u_\tau$. The grid resolution in wall units is chosen according to the following wall-resolved criteria [9].

- Chordwise : $dx^+ = \frac{dx}{y^+} \sim 50 - 130$; where $y^+ = \frac{y u_\tau}{\nu}$ and $u_\tau = \sqrt{\frac{\tau}{\rho}}$,
- Wall-normal : $dy^+ \sim 1 - 2$ ,
- Spanwise : $dz^+ \sim 15 - 40$;

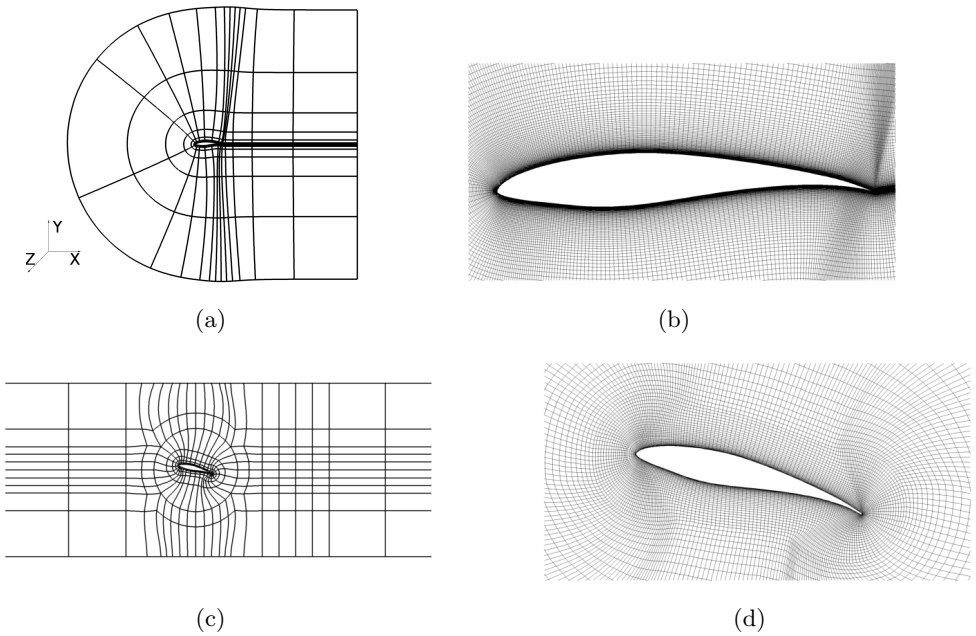


**Figure 2:** Computational domain using (a,b) the C-mesh, and (c,d) the Tunnel mesh. The bold lines represent the edges of each computational block.

where the small letters *(x,y,z)* denote the chordwise, wall-normall, and spanwise directions on the airfoil surface. This range of grid spacing requires a highly-resolved near-wall resolution. On the other hand, a large span to chord ratio is needed to resolve the stall cells accurately. Therefore a balance is required between the number of mesh points in the spanwise direction and the span-to-chord ratio. From previous studies, it has been found that the effect of spanwise resolution is more important than the span width and that a span to chord ratio of at least 0.12 should be used to predict proper 3D flow features [11]. In this paper, the spanwise resolution requirements are preferred to the span width. In two cases, however, highly resolved simulations with aspect ratio of $s/c = 1$ is used. A homogenuous free-stream turbulence with an intensity of 0.2% is introduced at $1c$ upstream of the airfoil to mimic the free stream turbulence of the tunnel. Simulations are run for at least two NTUs[1] and the statistics are averaged for approximately four NTUs to ensure that the statistics are converged. Table 1 shows a description of different test cases.

[1] Non-dimensional Time Unit $NTU = c/u_0$ is calculated as the time it takes for a flow particle to pass the airfoil chord

**Table 1:** Simulation setup for the airfoil LES computations.

| *Mesh type* | $\alpha^o$ | $Re$ | $N_\zeta \times N_\eta \times N_z^\dagger$ | $s/c$ |
|---|---|---|---|---|
| *C* | -6 to 4$^\ddagger$ | 100,000 | $960 \times 320 \times 64$ | 0.5 |
| *Tunnel* | 6 to 20$^\ddagger$ | 100,000 | $1024 \times 256 \times 64 - 320^\star$ | [0.12 1] |

$^\dagger$ Chordwise, wall normal, and spanwise resolution, respectively.
$^\ddagger$ A range of AoAs with steps of 2 degrees was performed.
$^\star$ Different spanwise resolutions corresponding to different span widths are used.
$^\star$ Unless otherwise stated explicitly, $s/c = 0.12$ and $N_z = 64$ is used for all computations.

## 4. Simulation results

This section presents a comparison of the pressure distribution as well as lift and drag coefficients obtained from LES computations with the wind tunnel measurements for a range of angles of attack and Reynolds numbers [2]. The instantaneous streamwise velocity and turbulence kinetic energy contours are plotted in figure 3 for $Re = 100,000$ at $\alpha = 12^o$. A grid resolution of $1024 \times 256 \times 64$ with an aspect ratio of 0.12 is employed. As can be seen, contours of the TKE show a peak of turbulence at the separation point which is decreased downstream until the wake recovers.

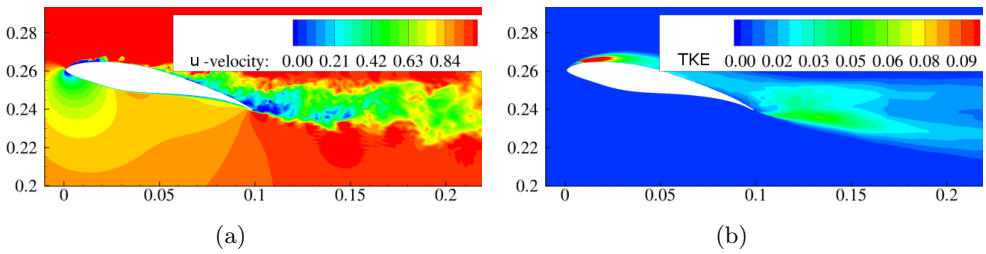


(a) (b)

**Figure 3:** Snapshots of (a) instantaneous streamwise velocity, (b) resolved turbulence kinetic energy for $Re = 100,000$ at $\alpha = 12^o$.

### *4.1. Comparison of pressure distribution over the airfoil*

This section presents pressure distributions on the airfoil for different angles of attack incremented from $\alpha = -8^o$ to $\alpha = 20^o$. Figure 4 shows the pressure distributions for $\alpha = -6^o, -2^o, 0^o, 2^o$. As can be seen, a reasonably good agreement between LES computations and the measurements is obtained over the entire airfoil surface.

The $C_p$ distributions for the positive angles of attack of $6^o$, $8^o$, $10^o$, and $20^o$ are plotted in figure 5. For $\alpha = 6^o$, the LES data show close similarity in the magnitude of the peak

[2] For the measurements, the error bounds are calculated based on the standard deviation of the measured pressure distribution and it is found that the maximum uncertainties are less than 1% of the mean values, with higher uncertainties close to the LE on the upper surface of the airfoil.

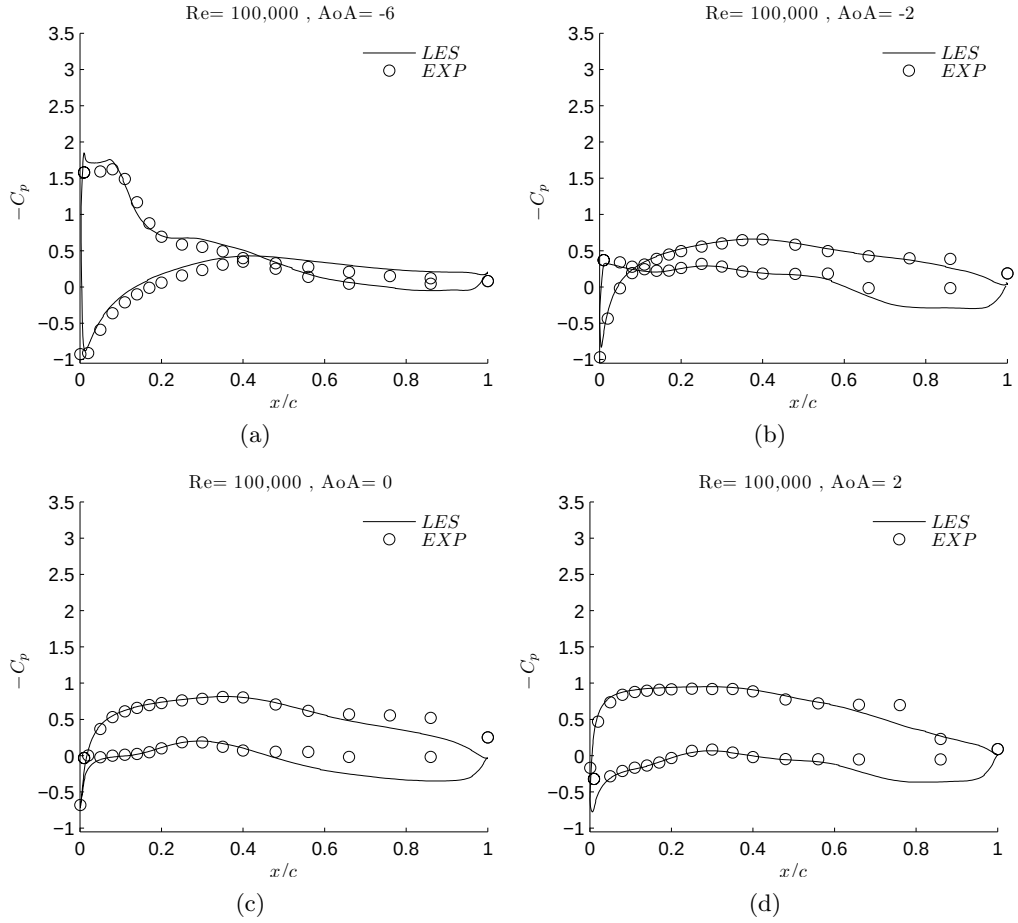


**Figure 4:** Comparison of $C_p$ for Re=100,000 at $\alpha = -6^o, -2^o, 0^o,$ and $2^o$.

pressure and pressure distribution for up to half a chord length downstream of the LE while the experimental data exhibit a separation at $x/c \sim 0.7$ which is not captured in LES due to unability of the numerical method in finding the exact transition location. This is most likely due to the inability of the SGS model and/or a slight inconsistency between the free-stream turbulence levels in the experiments and numerical simulations. The closest match between LES data and the measurements is obtained at $\alpha = 8^o$ where the pressure distribution falls on top of the measurements at all angles of attack.

At $\alpha = 10^o$, as shown in figure 5, LES shows a separation point starting at $x/c = 0.1$ and reattaching at $x/c = 0.4$. From figure 5(d), it is seen that the pressure distribution at $\alpha = 20^o$ is also in good agreement with the measurement data [3].

[3] As can be seen from figure 5(d), the numerical $C_p$ distribution for $\alpha = 20^o$ does not go from 0 to 1 unlike the other cases and the measurements. This is because a coarse grid is used which does not have

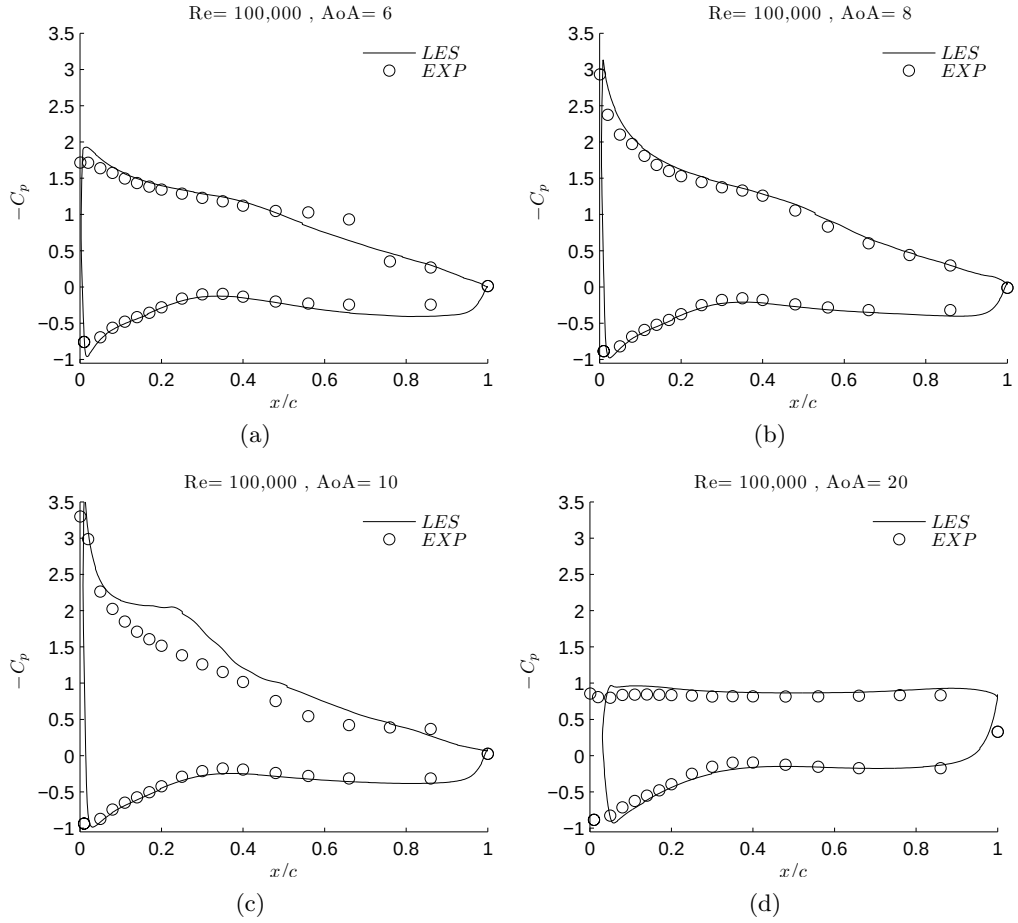


**Figure 5:** Comparison of $C_p$ for Re=100,000 at $\alpha = 6^o, 8^o, 10^o,$ and $20^o$.

*4.2. Comparison of lift and drag polars*

The final investigation is obtained between the time-averaged lift and drag polars predicted with LES and compared with experiments. Lift and drag coefficients are calculated by integrating the pressure forces and the skin friction on the airfoil,

$$C_L = \frac{F_{py} + F_{\nu y}}{0.5\rho U_0^2 cs} \ , \quad C_D = \frac{F_{px} + F_{\nu x}}{0.5\rho U_0^2 cs}. \tag{2}$$

where $F_{py}$ and $F_{px}$ are the pressure force in the vertical and streamwise directions. Similarly, $F_{\nu y}$ and $F_{\nu x}$ are viscous forces in vertical and streamwise directions. $c$ and $s$ are the chord and span lengths, respectively. For the experiments, the lift is obtained

a grid point in the LE.

directly from the force gauge measurement and the drag is calculated based on the integration of the wake profiles.

Figure 6 shows the lift and drag comparisons for the LES versus experiments. The experiments performed by Sarmast [20] is also included. As can be seen, LES computations agrees with the measurements for pitching angles up to $\alpha = 8^o$ although LES tends to over-predict the lift coeficients. The numerical simulations start to deviate from the measurements at higher angles of attack. Another difference is that the deep stall for numerical simulations occur at $\alpha \sim 12^o$ while the experimental results suggest an earlier stall. The differences between LES results and the measurements can most likely be explained by the inability of the LES to find the exact location of the transition point with the given numerical set-up, including the limitations of the chosen SGS model, numerical discretization schemes, and the limited span width ($\frac{s}{c}|_{numerical} = 1$ versus $\frac{s}{c}|_{experimental} = 5$).

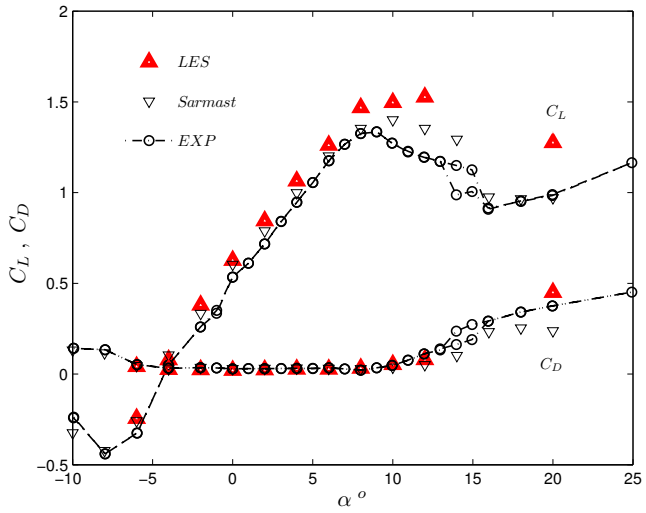


**Figure 6:** Comparison of lift and drag polars for Re=100,000.

Similar to the lift coefficients, the LES and the experimental results exhibit a good agreement between the $C_D$ polars for the low values and the differences appear in higher angles of attack. At $\alpha \geq 15^o$, while the accuracy of the current measurements is higher than those made by Sarmast [20] (due to the more accurate measurement equipment), the reliability of measurements is lower than at smaller pitching angles. This is because the drag is computed using the wake deficit and at high angles, the wake rake in the current set-up is not wide enough to capture the whole wake profile accurately.

## 5. Conclusion

In this paper, wind tunnel measurements and LES of the S826 airfoil were presented and lift and drag polars as well as pressure distributions on the airfoil surface were obtained at a Reynolds number of $Re = 100,000$ for different angles of attack. An LES study was also performed, in which the pressure distribution as well as lift and drag polars obtained using the LES computations were compared with the wind tunnel measurements. For the LES computations, a mixed scale SGS model was used and no explicit treatment was applied for the transition point. The lift and drag polars from the numerical simulations were found to be in acceptable agreement with the measurement, although at high angles of attack, the numerical computations over-predict the lift coefficients. As a general conclusion, it has been shown that LES is capable of capturing the main features of flow around the airfoil in terms of lift and drag polars as well as pressure distribution.

## References

[1] Anderson, JD 1998 *A history of aerodynamics: and its impact on flying machines*. Vol. 8. Cambridge University Press.

[2] Selig MS Donovan JF and Fraser DB 1989 *Airfoils at low speeds* HA Stokely.

[3] Somers DM. 2005 *The S825 and S826 Airfoils*, NREL/SR-500-36344.

[4] Uranga A et al. 2009 Implicit large eddy simulation of transitional flows over airfoils and wings. *Proceedings of the 19th AIAA Computational Fluid Dynamics, no. AIAA 4131.*

[5] Windte, J et al. 2004 RANS simulation of the transitional flow around airfoils at low Reynolds Numbers for steady and unsteady onset conditions. Tech. Univ. Braunschweig report.

[6] Michelsen JA 1992 *Basis3D- A platform for development of multiblock PDE solvers*, Technical report AFM 92-05, Tech. Univ. Denmark.

[7] Sørensen NN 1995 *General purpose flow solver applied to flow over hills*, Risø-R-827-(EN), RisøNational Laboratory, Denmark.

[8] Sarlak H 2014 *Large Eddy Simulation of Turbulent Flows in Wind Energy*, PhD Thesis, Tech. Univ. Denmark.

[9] Piomelli U, Benocci C and van Beek J 2012 *Large eddy simulation and related techniques: Theory and applications* Von Karman Institute Lecture Series ISSN 0377-8312.

[10] Davidson L 2003 *LESFOIL: Large Eddy Simulation of Flow Around a High Lift Airfoil*. Vol. 83. Springer.

[11] Mellen, CP et al. 2003 Lessons from LESFOIL project on large-eddy simulation of flow around an airfoil *AIAA journal* 41.4 pp. 573-581.

[12] Lenormand E Sagaut P, and Ta Phuoc L. 2000 Large eddy simulation of subsonic and supersonic channel flow at moderate Reynolds number. *International Journal for Numerical Methods in Fluids* 32.4 pp. 369-406.

[13] Sagaut P 1995 *Simulations num eriques d ecoulements lecoll les avec des mod'eles de sous-maille* PhD thesis, Univ. Pierre et Marie Curie.

[14] Winkelman, AE, and Jewell BB 1980 Flowfield model for a rectangular planform wing beyond stall *AIAA Journal* 18.8 pp. 1006-1008.

[15] Mary I, and Sagaut P 2002 Large eddy simulation of flow around an airfoil near stall. *AIAA journal* 40.6 pp. 1139-1145.

[16] Venugopal, P et al. 2012 Large eddy simulation of a wind turbine airfoil at high angle of attack. *Proceedings of the Summer Program*, Stanford University.

[17] Rhie, CM, and Chow WL 1983 Numerical study of the turbulent flow past an airfoil with trailing edge separation. *AIAA journal* 21.11 pp. 1525-1532.

[18] Ying Z and Wang ZJ 2010 Implicit large eddy simulation of transitional flow over a SD7003 wing using high-order spectral difference method. *AIAA Journal* 4442.

[19] Schlichting H 1955 *Boundary-layer theory*. McGraw-Hill.

[20] Sarmast S 2013 *Numerical study on instability and interaction of wind turbine wakes*. Lic. Thesis, Trita-MEK KTH, Stability, Transition and Control 2013:08.

[21] Eisenbach S and Friedrich R 2008 Large-eddy simulation of flow separation on an airfoil at a high angle of attack and Re=$10^5$ using Cartesian grids. *Theoretical and Computational Fluid Dynamics* 22.3-4 pp. 213-225.